DESIGN OF MINIMUM VOLUME EMC INPUT FILTERS FOR AN ULTRA COMPACT THREE-PHASE PWM RECTIFIER

Marcelo L. Heldwein and Johann W. Kolar

Swiss Federal Institute of Technology (ETH) Zurich
Power Electronic Systems Laboratory
ETH Zentrum / ETL H.23, Physikstrasse 3
CH-8092 Zurich / SWITZERLAND / Europe
heldwein@lem.ee.ethz.ch   kolar@lem.ee.ethz.ch

Abstract—A design procedure is proposed for the EMC filters to be included in a three-phase/-level PWM rectifier unit in order to fulfill EMC requirements related to conducted emissions. An analytical volumetric optimization is performed considering constraints given by electrical safety, power factor and damping of resonances. The procedure avoids the necessity of applying numerical optimization allowing the analytical calculation of the total filter volume as function of rated power and switching frequency. A discussion about the limits of power density for the rectifier employing modern power semiconductors is done and optimum switching frequency of 540 kHz is calculated for a forced air-cooled system. The experimental verification of the proposed procedure is presented through CE measurements in the designed system.

Keywords—Input filter, Minimum volume filters, Three-phase filter design, Ultra-Compact Rectifier.

I. INTRODUCTION

The demands for higher system compactness have moved Power Electronics research towards the limits of available circuit topologies, materials, components, modulation schemes and control strategies [1]–[2]. Increasing switching frequencies, newly developed materials and high performance cooling systems have allowed the miniaturization of the power converters, which consequently present electromagnetic field spectra of higher frequencies confined to smaller spaces [2]–[4], where one component notably influences the other if attention is not put on their physical disposition. As electromagnetic compatibility (EMC) must obviously be guaranteed inside the system and within its environment [5], electromagnetic emissions control strategies should be employed. For the reduction of conducted emissions (CE), filters have been designed and applied as an interface between the electrical power grid and the power electronics converters. For high performance three-phase rectifier systems, these input filters are typically designed based on passive components, inductors and capacitors along with resistors providing passive damping [6]–[7]. These passive filters are responsible for a significant part of the power system's volume and many efforts have been made in order to improve the performance of filter components and to develop filter topologies allowing for volume, size and costs reduction. There, multi-stage LC filters lead to more compact filters and sometimes cheaper than single-stage ones [8].

To contribute on this subject a design structure is proposed, which allows for efficient designing compact EMC input filters for a three-phase/-level PWM rectifier, which is employed as a power factor correction (PFC) front-end converter in telecommunication power supplies. The converter power circuits are shown in **Fig. 1** [8]. This rectifier
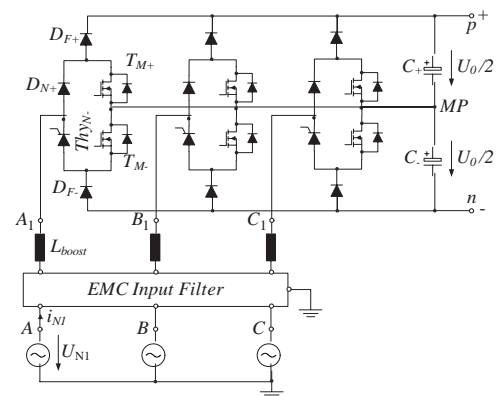

Fig. 1: Circuit schematic of the 3-phase, 6-switch, 3-level Vienna Rectifier topology used to implement the 10 kW PWM rectifier.

has an output power of 10 kW, power density of 8 kW/dm^3, switching frequency f_p=400 kHz, output voltage U_o=760 V, input voltage U_{N1}=230 V and is forced air-cooled. The EMC filter is designed to fulfill EMC requirements, where an attenuation specification, based on the estimated CE levels of the rectifier, is calculated. Furthermore, the filters are designed taking into account the limits for CE specified for Class B information technology (IT) equipments as in CISPR 22. The aim is that the designed filters are of minimum volume, present the required attenuation characteristics for the frequency range of interest and included passive damping networks, leading to reasonable efforts for the control design.

The proposed procedure has its emphasis on the minimization of the total filter volume through analytical considerations, avoiding the necessity of numerical optimization calculations [11]–[13]. The design of the filters is then split into two tasks, common mode (CM) and differential mode (DM) filter designs. These tasks are performed before a prototype is built, based on simplified frequency spectra and numerical simulation results of the rectifier and different equivalent circuits for each of the noise modes.

Being the proposed procedure based on analytical equations, a study about the influence of the switching frequency and the parasitic capacitances on the total filter volume is possible. Such study is performed for the rectifier at hand. The results show the impact of the EMC filter volume in the achievable power density.

This paper is structured as follows. **Section II** presents the requirements for the filter design along with design assumptions and the input data, namely the frequency spectra of interest and the characteristics of the boost inductors. The definition of the CM filter design is shown in **Section III**, with emphasis in the selection of materials and compo-
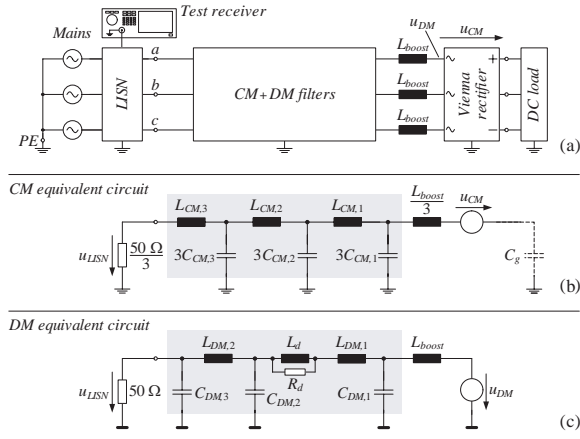
Fig. 2: (a) CE test setup and filter topologies with their simplified equivalent circuits for (a) CM, and; (b) DM.

nents. The DM filter design procedure is presented in **Section IV**, where the assumptions used in the design and the detailed choice of components are given. The study about the influence of switching frequency and parasitic capacitances is presented in **Section V**. **Section VI** illustrates the experimental results achieved for the three-phase 400 kHz rectifier by presenting the final filter structure and CE measurements according to CISPR 22. Finally, conclusions and an outlook for future research are presented, showing the necessity of further improving the CE DM filtering techniques, since power densities of 50 kW/dm^3 are to be expected in the next years [14] bringing even tougher demands for input filters.

II. EQUIVALENT CIRCUITS AND REQUIREMENTS

The design procedure starts by defining equivalent circuits used to evaluate CM and DM noise sources and to design appropriate filtering circuits. As the prime objective of the filtering circuits is to reduce emissions at frequencies typically lower than 1 MHz, the definition of very accurate models, including higher order parasitics as magnetic and capacitive couplings among components and PCB impedances, is not mandatory as long as safe margins are respected. The uncertainties in obtaining very precise simulation models, which include most of the parasitic effects observed in a prototype, also supports this practice. These parasitic impedances are critical for the filter layout and components construction, but are not essential for the input filter design. For these reasons, the circuits presented in **Fig. 2** are employed in this work, where the voltages u_{CM}, u_{DM}, the inductors L_{boost} and the capacitance C_g model the power converter CM and DM noise source circuits.

Capacitance C_g is a lumped representation of all stray capacitances from the power circuit and load to the protective earth (PE). Not considering load and assuming that the heatsink is bonded to PE, C_g represents mainly the capacitances from the semiconductors to the heatsink. Typically, impedance C_g is distributed and presents resistive and inductive portions. Thus, one capacitor at the output of the rectifier represents worst-case except from strong resonances, which are possible at higher frequencies. The maximum value calculated for the capacitances from the power semiconductors is around 300 pF, typical capacitances from test loads are in the range 200 pF to 2 nF. The value used for the design is C_g=2 nF. Higher capacitances between load and PE are not specifically considered, since a CM choke can be used at the DC-link terminals [15] limiting the influence of any DC load. Inductors L_{boost} model the input inductors of the rectifier, which influence CM and

DM current paths. Impedance measurements of the built inductors show an inductance of approximately 30 μH and a self-resonance frequency around 8.5 MHz.

The design of the filters is performed in the frequency domain, since the required attenuation is defined in terms of frequency and suitable impedance models for the filtering components are at hand for this domain. Therefore the estimation of frequency spectra for DM and CM voltages and/or currents is required. A simple simulation with ideal devices presenting rise and fall times close to zero and without the inclusion of parasitic elements is able to provide spectra which are conservative, except at the frequencies close to the characteristic frequencies related to the rise and fall times due to over-voltages and oscillations. Another point which can be neglected in this simulation is the inclusion of the LISN circuits, once the voltage spectra do not sensibly change. At last the circuit is considered to be perfectly balanced. The simulation circuit can be as in Fig. 1 except that the EMC filter is removed and the switches are replaced by ideal ones. For the power converter at hand, the boost inductors are included in the simulation as ideal inductors, but are also seen as part of the input filters. The spectrum of the input currents change with the inclusion of the other filter components and, for that reason, the input currents spectra are not used for the design of the filters.

For the CM design the relevant spectrum is of the voltage between the DC-link center point MP and the terminals A_1, B_1 and C_1 with the CM voltage u_{CM} given by,

$$u_{CM} = u_{MP} - \frac{u_{A1} + u_{B1} + u_{C1}}{3}. \tag{1}$$

Considering symmetrical spectra for the three phases, the DM filter the spectrum of interest is one of the DM voltages at terminals A_1, B_1 and C_1. The DM voltage u_{DM} is taken for phase A as,

$$u_{DM} = \frac{2}{3}u_{A1} - \frac{1}{3}u_{B1} - \frac{1}{3}u_{C1}. \tag{2}$$

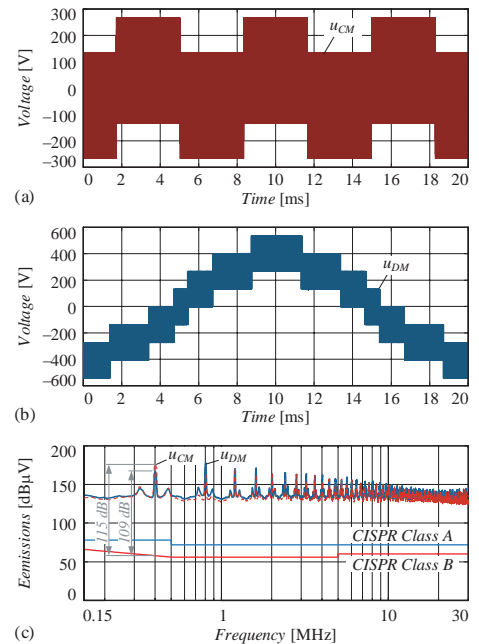These spectra are compared to the limits at the frequency

Fig. 3: Waveforms and spectra from the rectifiers' simulation results: (a) Time behavior of the CM voltage u_{CM}; (b) Time behavior of one of the DM voltages u_{DM}; (c) Conducted emissions predicted spectra for both voltages for the worst case QP detection (linear sum of the harmonic inside the resolution bandwidth) [17].
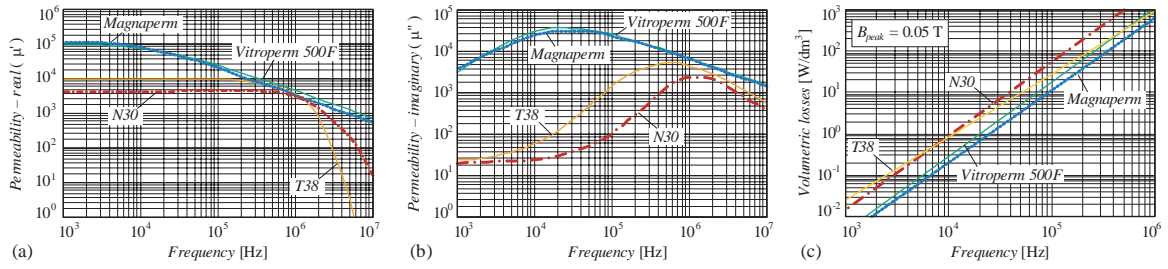
455

Fig. 4: Properties of different core materials suitable for CM inductors: (a) Real part of complex permeability; (b) Imaginary part of complex permeability; (c) Volumetric losses in dependency of frequency for a peak flux density of 50 mT.

of interest f_{int} which is 150 kHz for switching frequencies lower than 150 kHz or the switching frequency for higher frequencies. This gives the required attenuation, Att_{req}, at the frequency of interest,

$$Att_{req,CM/DM}(f_{int}) = 20 \cdot \log\left[\frac{U_{CM/DM}(f_{int})}{1 \,\mu V}\right] - Limit(f_{int}) \,. \qquad (3)$$

The simulation results are presented in **Fig. 3** for nominal conditions, which, as required by the CE test specifications [16], is the worst-case emission condition since the fastest rise and fall times are observed for voltages and currents. Fig. 3(a) shows the time behavior of u_{CM}, which is composed of voltage steps with a value of $\pm U_o/6$ and presents a strong third harmonic component with respect to the mains frequency. The differential voltage u_{DM} is plotted in Fig. 3(b) and is responsible for the sinusoidal shaping of the input currents with voltage steps of $\pm U_o/6$ and $\pm U_o/3$.

The design must also take into account the specified CE measurement, which in this case is done with two types of detector, the quasi-peak (QP) and average (AVG), presenting both non-linear behavior. For this work, only the QP detector is considered and its behavior is modeled as proposed in [17], by linearizing it. Accordingly, the voltage spectra shown in Fig. 3(c) account for a maximum value for the QP measurement, which leads to slightly over dimensioned filters, but as uncertainties, such as components tolerances, are present this is seen as an advantage. It is observed that, at f_s=400 kHz, both spectra present the worst condition for the filter design task and attenuations of:

$$\begin{aligned} Att_{req,CM} &= -115 \text{ dB @ } f_s = 400 \text{ kHz} \\ Att_{req,DM} &= -109 \text{ dB @ } f_s = 400 \text{ kHz} \end{aligned} \qquad (4)$$

are required in order to fulfill CISPR 22 Class B requirements with a 6 dB margin.

III. CM FILTER DESIGN

The first task in the CM filter design is to choose an appropriate filter topology. These filters are typically built with inductors and capacitors in a low-pass arrangement, which can have many stages and different configurations. Multi-stage filters have the potential to lower the total filter size and costs. Reference [8] defines the conditions and requirements at which each topology presents an advantage. For the case at hand, a three-stage topology is presented in Fig. 2(b) in its single-phase equivalent.

Two main components are used in the CM filter, coupled inductors and capacitors. Equipment safety regulations [18] play an important role, since restrain the allowable earth leakage current; define requirements for capacitors between an input line and PE, and; define insulation requirements for CM inductors and filter construction.

Earth leakage current $I_{PE,rms,max}$ is typically limited to 3.5 mA, even for the case where one of the phases is lost. Thus, the total capacitance $C_{CM,sum}=\Sigma C_{CM,i}$, i=1...3, between any

of the input phases and the PE is bounded to a maximum of approximately,

$$C_{CM,sum} \le \frac{I_{PE,rms,max}}{1.1 \cdot U_{N1,max} \cdot 2\pi \cdot 50 \text{ Hz}} \cong 44 \text{ nF} \,. \qquad (5)$$

Safety also requires Y2 rated capacitors. Due to these restrictions a series of Y2 ceramic capacitors [19] is chosen, which presents a maximum capacitance of 4.7 nF per SMD package, leading to compact construction and low parasitics. Since other capacitances are present in the circuit (arrestors, stray capacitances, etc) and values present tolerances, some margin is provided so that $C_{CM,sum}$=7·4.7 nF=32.9 nF, to be divided in the filter stages. According to Section IV, for maximum attenuation given a minimum total capacitance, each stage shall present the same value. The final configuration and chosen components are shown in Section VI.

The other elements of the CM filter are the coupled inductors [20]. These are designed based on their required impedance at a given frequency because core magnetic materials present a non-constant complex permeability with frequency. An imaginary part μ'' increases the total impedance and the CM choke behaves as a series RL connection. The proper choice of core materials leads to compact and effective inductors, with reduced parasitics. The main characteristics for CM reduction for some popular and high performance magnetic materials are shown in **Fig. 4**. Two types of ferrite (N30 and T38), a nanocrystalline (VITROPERM 500F) and an amorphous material (MAGNAPERM) are compared. It is observed that the real part of the permeability of all materials is similar in the 0.2 to 2 MHz range, but the non-ferrite materials present higher permeabilities for other frequencies. The imaginary part is lower for ferrites. Even core losses are higher for these ferrites. Core losses are usually not considered when designing CM chokes, but when high switching frequencies (400 kHz for this design) are employed, this shall be considered. The maximum flux density are $B_{sat,VITROPERM} \cong 1.2$ T, $B_{sat,MAGNAPERM} \cong 0.6$ T, while it is lower than 0.3 T for the ferrites. This comparison shows that CM inductors can be smaller by applying materials with high permeability and saturation point. Given these reasons, VITROPERM 500 F is chosen for the CM chokes. This material presents good thermal stability as well.

To design the inductors, a complete model is used, based on a series of designs. A series of inductors are designed with the following assumptions:

– possible asymmetries, parasitic capacitances and the effect of the tolerances are neglected;
– ambient temperature equals 45°C and the maximum temperature rise is 60 °C;
– a single winding layer is allowed in order to reduce parasitics;
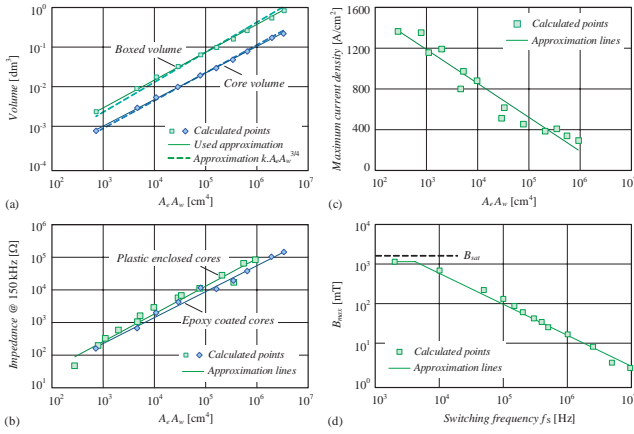– iterative choice of the maximum flux density B_{max} and current density J_{max} is performed;

Fig. 5: CM inductor design curves for core material VAC VITROPERM 500F: (A) Dependency of an inductor's boxed and core volume on area product $A_e A_w$ of the used material. (b) Impedance at 150 kHz and 15 A_{RMS} as a function of area product for two core types namely, epoxy coated cores and cores with a plastic enclosure. (c) Maximum current density as a function of the area product. (d) Maximum flux density as a function of the switching frequency.

– discrete values determined by the limited choice of cores and wire diameters are approximated by continuous functions.

Based on these design guidelines, a series of inductor designs is conducted for different frequencies and current ratings. The results are summarized in **Fig. 5**. Based on the performed designs, Fig. 5 presents the used maximum current density J_{max} (Fig. 5(a)) and flux density B_{max} (Fig. 5(b)) as functions of the core product of areas $A_e A_w$ and switching frequency f_s, respectively. In Fig. 5(a) the dependency of the volume of an inductor to its product of areas $A_e A_w$ is depicted along with the core volume. This dependency is usually considered with a power of 3/4, but for the case at hand a lower factor is used leading to closer approximations. Finally, based on these considerations and on the material's complex permeability curves an equation for the maximum achievable CM choke impedance Z_{choke} for a given product of areas and switching frequency is empirically derived,

$$Z_{choke}(f_{int}) \cong 10^{2.243 - 2 \cdot \log(I_{N1}) + 0.181 \cdot \log(|\mu(f_{int})| \cdot f_{int}) \cdot \log(A_e A_w)} . \quad (6)$$

Equation (6) presents an R-squared value higher than 0.939 for frequencies in the range 150 kHz $\leq f_{int} \leq$ 10 MHz, when compared with the calculated values. Solving (6) for the product of areas leads to the core size and its volume can be calculated with the help of the curves depicted in Fig. 5(c). This approach is useful in an optimization procedure where a minimum total volume for the filters and power converter are searched. Considering empirically approximated voltage spectra envelopes, all filter parameters can be defined as a function of the switching frequency. As an example, **Fig. 6** shows the dependency of the CM filter volume as a function switching frequency f_s and total ca-
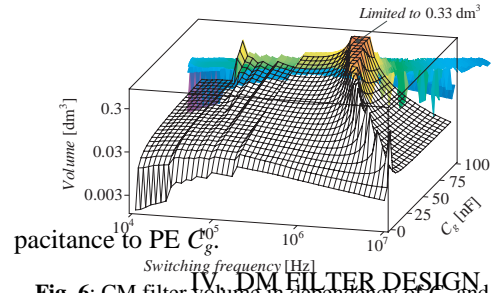

Fig. 6: CM filter volume in dependency of C_g and f_s.

pacitance to PE $C_g^{0.5}$

IV. DM FILTER DESIGN

The filter topology used for the DM design is shown as a single-phase equivalent in Fig. 2(c). Three-stages are chosen based on power and attenuation [8]. Components are chosen based on a series of requirements and aiming for the smallest total volume.

Safety regulations [18] mainly define the capacitors connected between lines. Besides that, the inclusion of the filter generates a displacement in the input currents. Assuming that the rectifier presents resistive behavior and that the and inductors are low impedances at the line frequency, at light load the capacitive currents drained by the capacitors generate leading currents in the mains and a limit for the displacement angle constrains the maximum capacitance value. In this work, the maximum input current displacement angle $\Phi_{in,max}$ is set to $\Phi_{in,max}$=5° for an output power of 10%, what means a power factor higher than 0.995.

Minimum inductance for the boost inductors is required for the normal operation of the rectifier. For this design the allowable switching frequency ripple is $\Delta i_{boost,max}$=25% of the peak input current $I_{N1,peak}$. High frequency losses can not be neglected and the design aims in minimizing overall losses. A calculation of the optimal point can be done [21] and is omitted for the sake of brevity.

The design of the DM inductors is considerably different than that of the CM ones. The DM currents are composed of a high mains frequency component and a relatively small high frequency ripple due to the attenuation given by the boost inductors and capacitors $C_{DM,1}$. For this reason, the cross sectional area of the core A_e is determined by saturation and not by core losses. Furthermore, the high frequency losses in the winding are also comparatively small and can be neglected. The other parameter that defines the core is the required winding area A_w.

The filter inductance $L_{DM,i}$ and rated current are related to the size of the inductor $A_e A_w$ (core area product) by

$$L_{DM,i} I_{N1,peak} I_{N1,rms} = k_w J_{max} B_{peak} A_e A_w . \quad (7)$$

The volume of the filter inductor V_L is calculated with

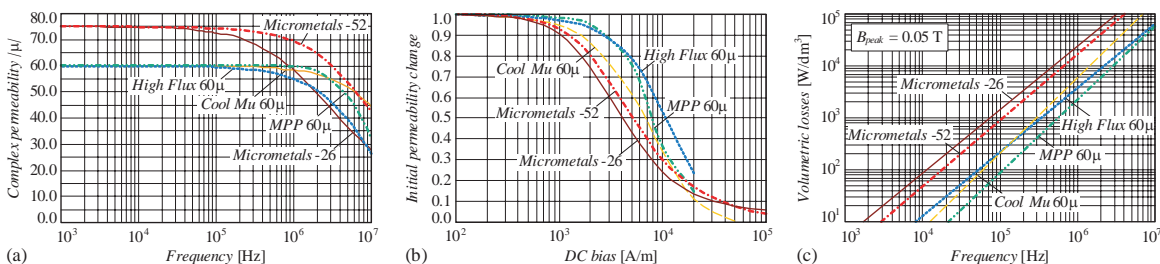$$V_L = k_{geo}(A_e A_w)^{\alpha_{geo}} . \quad (8)$$

Fig. 7: Properties of core materials for DM inductors: (a) Magnitude of the complex permeability versus frequency; (b) Per unit change in permeability in dependency of the DC bias; (c) Volumetric losses in dependency of frequency for a peak flux density of 50 mT.

There, the parameters k_{geo} and α_{geo} account for the geometry of the core (toroidal, planar, etc). Assuming that a dimension grows proportionally with the other ones, α_{geo} is usually taken as 3/4.

To choose appropriate material for the cores a comparison of core materials is done for different types of iron powder materials in their standard permeability values (cf. **Fig. 7**). These materials present a saturation flux density B_{sat} much higher than for ferrites allowing for smaller inductors and reduced number of turns. From Fig. 7(a) it is seen that KoolMu and Molypermaloy (MPP) present the lower relative reduction of permeability with increasing frequency. Fig. 7(b) shows that High Flux has the lowest permeability reduction with higher magnetic field values. MPP outperforms the other materials in the high frequency losses (Fig. 7(c)) and maximum operating temperature [22]–[23]. Nevertheless, High Flux presents a very high saturation flux $B_{sat} = 1.3$ T, which is 30 % to 70 % higher than any of the others. For this reason, this material is chosen in order to achieve the lowest volume inductors. A series of designs is performed aiming for a characterization of the volume of the DM inductors related to their rated current and inductance. The resulting designs are shown in **Fig. 8**(a), suggesting that the volume of this type of inductor is proportional to its stored energy.

The volume of the capacitors to be used in the filters is approximated by a curve generated by Minimum Square fitting of the volumes calculated for commercially available X2 type capacitors [19] and [24] as well as for ceramic capacitors rated for the Japanese mains [19]. The approximation curves along with the calculated values for discrete capacitors are presented in Fig. 8(b) and also suggest a volume dependency with the stored energy.

Assuming that the volume of the components is directly related to their stored energy, the volumetric coefficients for inductors k_L and capacitors k_C are defined as in

$$V_{L,i} = k_L \cdot L_{DM,i} \cdot I_{N1}^2 \text{ and } V_{C,i} = k_C \cdot C_{DM,i} \cdot U_{N1}^2 . \tag{9}$$

These coefficients are derived as shown in Fig. 8. Two equations define the minimization problem, the attenuation at the frequency of interest f_{int}, that represents the main constraint, and the filter volume, which shall be minimized.

An asymptotic approximation of the attenuation Att, for frequencies much higher than the corner frequency, is used,

$$\frac{1}{Att(f_{int})} \cong \left(2\pi \cdot f_{int}\right)^6 \cdot L_{boost} \cdot \prod_{i=1}^{2} L_{DM,i} \cdot \prod_{i=1}^{3} C_{DM,i} . \tag{10}$$

It can be proven (cf. Appendix I) that for the lower total inductance, each of the individual inductors have the same value $L_{DM,i}=L_{DM}$ and this is valid for the capacitors $C_{DM,i}=C_{DM}$. Thus, two variables are left to minimize the volume. The required attenuation Att_{req} equation is simplified,

$$\frac{1}{Att_{req}} \cong \left(2\pi \cdot f_{int}\right)^6 \cdot L_{boost} \cdot L_{DM}^2 \cdot C_{DM}^3 . \tag{11}$$

The total volume of the filter is given by,

$$Vol_{DM} = 9 \cdot \left(Vol_L + Vol_D\right) + 3 \cdot Vol_{L_{boost}} . \tag{12}$$

Replacing (9) in (12),

$$Vol_{DM} = 9 \cdot \left(k_L \cdot L_{DM} \cdot I_{N1}^2 + k_C \cdot C_{DM} \cdot U_{N1}^2\right) + Vol_{L_{boost}} . \tag{13}$$

Rearranging (11) in terms of L_{DM} and replacing it in (13),

$$Vol_{DM} = \frac{9 k_L I_{N1}^2}{\left(2\pi f_{int}\right)^3 \sqrt{L_{boost} C_{DM}^3}} + 9 k_C C_{DM} U_{N1}^2 + Vol_{L_{boost}} . \tag{14}$$

The solution for a minimal volume is given for,

$$\frac{\partial Vol_{DM}}{\partial C_{DM}} = 0 . \tag{15}$$

The final values for the components are given by,

$$\begin{aligned} C_{DM} &= \frac{I_{N1}}{4\pi \cdot f_{int} \cdot U_{N1}} \cdot \sqrt[5]{\frac{36 \cdot k_L^2 \cdot U_{N1}}{\pi \cdot f_{int} \cdot L_{boost} \cdot Att_{req} \cdot k_C^2 \cdot I_{N1}}} . \\ L_{DM} &= \frac{U_{N1}}{6\pi \cdot f_{int} \cdot I_{N1}} \cdot \sqrt[5]{\frac{36 \cdot k_C^3 \cdot U_{N1}}{\pi \cdot f_{int} \cdot L_{boost} \cdot Att_{req} \cdot k_L^3 \cdot I_{N1}}} \end{aligned} \tag{16}$$

Requirements related to control issues must also be considered [25]–[26]. In order to provide passive damping that cause minimum losses and avoiding oscillations, RL networks are included in the choice of the topologies.

Thus, minimal volume filters can be designed based on the ratings of the components and the required filter attenuation assuming that parasitic elements do not strongly influence the attenuation at the frequency of interest, which is usually valid. This minimization procedure eliminates the need for a numerical optimization procedure [11]–[13], thus simplifying the design of minimum volume EMC filters.

The DM filter design procedure is presented in the block diagram of **Fig. 9**. It is seen that after the main components are defined and respect given constraints, damping is considered and the values of the leakage inductance of CM chokes is deducted from the required inductance to design the DM inductors.

Results for the proposed volume minimization procedure are depicted in **Fig. 10**. It is seen the volume and attenuation surfaces in dependency of the DM inductance L_{DM} and capacitance C_{DM}. The surfaces take into consideration a detailed model, with estimated parasitic elements (ESR, ESL, losses and parallel capacitance). These graphs are plotted for $k_L = 497.6 \cdot 10^{-6}$ m³·H⁻¹·A⁻² and $k_C = 32.7 \cdot 10^{-6}$ m³·H⁻¹·A⁻².

V. POWER DENSITY DISCUSSION

With the given volume minimization procedures for CM and DM filters the impact of the filter volume in the maximum achievable power density as a function of the
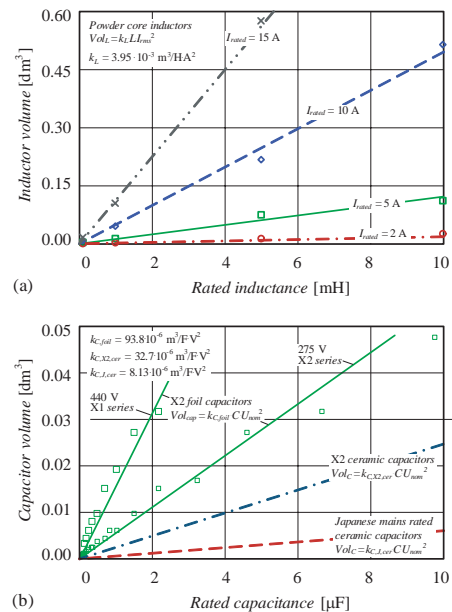

(a)

(b)

Fig. 8: Volume and volumetric coefficients of filter components. (a) Approximation of capacitors' volume for various mains rated types, X2 foil, X2 ceramics and Japanese mains rated ceramics. (b) Volume of toroidal Molypermalloy inductors in dependency of current and inductance value.
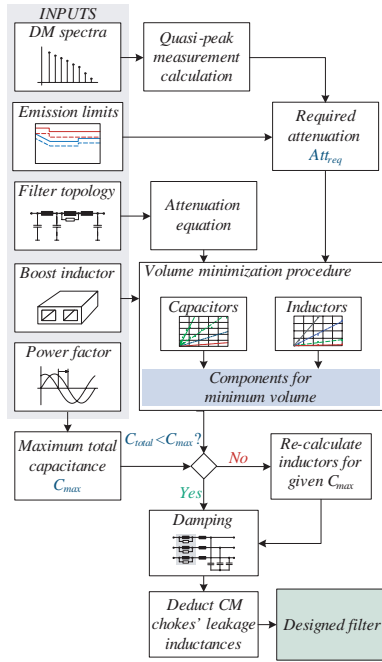
Fig. 9: Flowchart showing the input DM filter design procedure.

switching frequency is calculated and an optimum frequency can be estimated, aiming for maximizing overall power density. For the designed rectifier [9], a custom designed power module is employed. The calculated power losses as a function of switching frequency define a required thermal resistance for the cooling system. Based on that, the volume for an optimized forced air cooling systems is estimated [27]. For the calculations, a coefficient $CSPI$=25 W·K^{-1}·dm^{-3} [27] is used.

The design is performed for junction temperatures up to 125°C and ambient temperature of 45°C. A total capacitance to ground of C_g=2 nF is considered. The DM capacitors are X2 rated ceramics [19]. The estimated volumes are depicted in **Fig. 11**(a). It is seen that the DM filter (mainly the boost inductors) dominates the volume for low frequencies, whereas the CM is larger for higher switching frequencies. The increase in the switching losses is responsible for the large increase of the cooling system at high frequencies until it limits the feasibility of the rectifier for requiring negative thermal resistances. Fig. 11(b) presents the calculated power densities, for just the EMI filter and
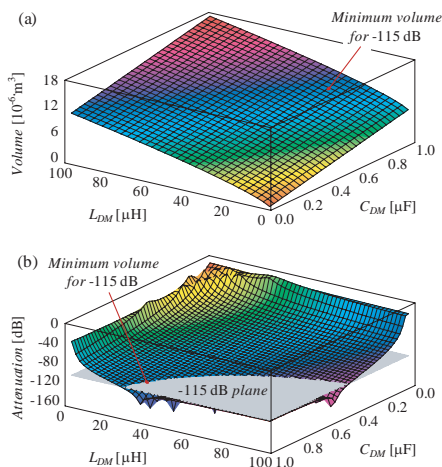

Fig. 10: Volume and attenuation surfaces for the DM filter design with Molypermaloy cores and X2 capacitors. (a) Volume dependence on L_{DM} and C_{DM} values; (b) Attenuation at f_s=400 kHz for L_{DM} and C_{DM} values and -115 dB plane (gray). Colors correspond to colors in (a).
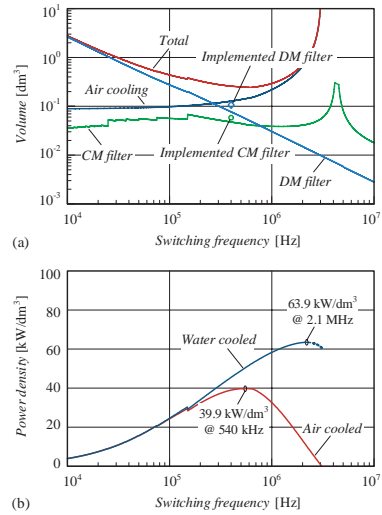

Fig. 11: EMC filters and cooling devices estimated (a) volume, with the final volume for the designed filters shown, and (b) power density in dependence of the switching frequency. The influence of the volumes of the CM and DM filter components, including the boost inductors and of the forced air cooling devices (fans and heatsink) is observed in the curves. The curves are generated for a total capacitance to ground of 2 nF. A curve for a possible water cooled system is added.

cooling system also for a water cooled system. A water cooled system is capable of further increasing the power density for high switching frequencies. For an air cooled system the higher power density is calculated as 39.9 kW/dm^3 for f_s≅540 kHz. This optimum frequency and the respective power density are further decreased with the inclusion of the other elements of the system and justify the choice for f_s=400 kHz.

VI. EXPERIMENTAL VERIFICATION

The rectifiers' construction views are shown in **Fig. 12**. The rectifier is designed for compactness. Thus, trade-offs among thermal, electrical, EMC and mechanical functions are required. The filter layout follows design rules to reduce interaction within filter elements and presents a straight line forward current flow. The current flows from the input terminals through the EMC filter, the current sensors and boost inductors, which links it to capacitor board. From this board the current flows through the power module into the output capacitors.

The schematic for the designed filter is depicted in **Fig. 13**, along with the specification of the filtering components. A comparison with the volume information achieved in Section V can be made leading to an error of 37 % for the DM filter components and 22 % for the CM ones. This is considered within the expected range arising from all simplifications made in the prediction procedure. Interesting
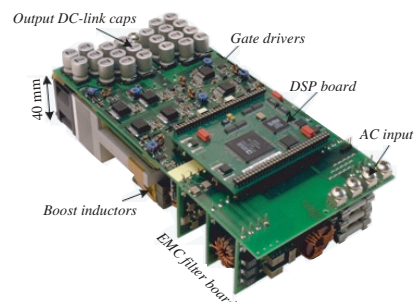

Fig. 12: Top view on rectifier with the EMC filter DSP board, gate drivers and electrolytic dc output capacitors.
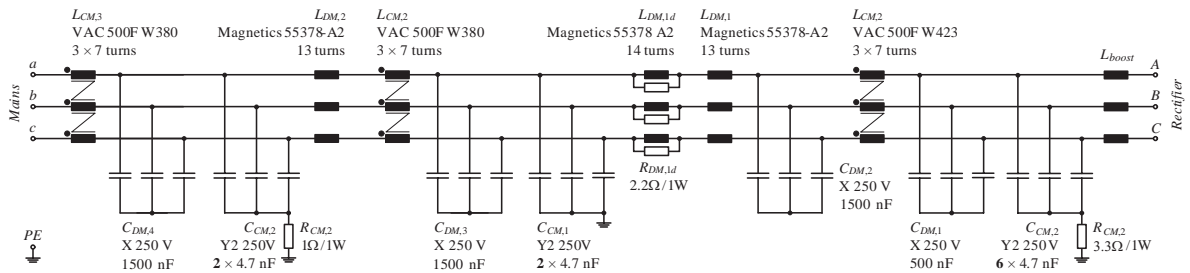
459

Fig. 13: Complete circuit schematic for the designed filter with the specifications of the main components.
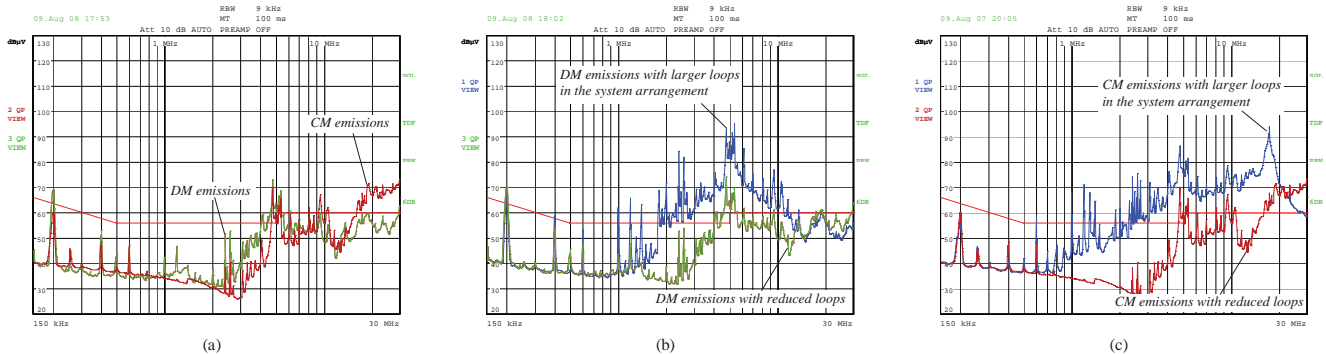

Fig. 14: First CE measurements. (a) Measured CM and DM emissions; (b) DM emissions for two different arrangements of the interconnections and placement of components for the same system and filter components, and; (c) CM emissions for two different arrangements.

information is that the final boxed volume of the complete filter is approximately 2.4 times larger than the sum of all individual components, meaning that interconnections, air and PCB account for nearly 60 % of the employed space. That leaves room for improvements through research on inter-components coupling reduction.

Due to thermal restrictions with the current cooling system, the switching frequency needed to be reduced to f_s=200 kHz. This will be increased in a redesign of the system.

Experimental results from conducted emissions (QP) measurements, according to CISPR 22, are shown in **Fig. 14**. A three-phase noise separator [28] has been used in order to allow the separate evaluation of DM and CM. Fig. 14(a) depicts the measured emission levels for CM and DM. For the DM emissions, the first harmonic is below the designed point (400 kHz) and, thus larger than predicted. These results are obtained in an open system, where no special shield was used. This explains for the worsening of the performance for higher frequencies. Nevertheless, the filter design procedure proves efficient since the components are designed for the switching frequency.

A comparison of the influence of cabling and grounding configurations in the emissions is presented in Fig. 14(b) and Fig. 14(c). DM emissions are shown in Fig. 14(b) for two different system configurations. CM emissions are presented in Fig. 14(c). It is seen that, for the same components and boards, the influence of the geometrical configuration of the interconnections and associated loops, is enormous. These effects can not be accounted for before hand in the proposed modeling, since they depend upon the 3-D geometry HF effects. This is the aim of future research, where parasitic modeling with field solvers are to be used in the design phase of a power system.

VII. CONCLUSIONS

This work proposes a design procedure for the EMC filters to be employed with a three-phase rectifier unit in order to fulfill CISPR 22 Class B requirements related to conducted emissions. The design procedure is explained; where a volumetric optimization is carried out taking into consideration different aspects related to the subject, such as electrical safety, power factor and damping of resonances. The presented procedure avoids the necessity of using numerical optimization routines and allows for the analytical calculation of the total filter volume as function of the rated power and switching frequency, therefore helping in the early determination of the optimum switching frequency for a given rectifier specification. A discussion about the limits of power density for the three-phase three-level PWM rectifier for a set of state-of-the-art power semiconductors is done and an optimum switching frequency of 540 kHz is identified for a forced air-cooled system. The experimental verification of the proposed filter design procedure is shown, where it is identified that the system physical configuration has a large influence in the final emissions performance. These effects shall be target for future research, so that computer aided design and virtual prototyping can be fully implemented.

REFERENCES

[1] F. C. Lee, and P. Barbosa, "The State-of-the-Art Power Electronics Technologies and Future Trends," in *Proc. IEEE PES Transmission and Distribution Conf. and Exp.*, vol. 2, 2001, pp.1188-1193.

[2] J. W. Kolar, U. Drofenik, J. Biela, M. L. Heldwein, H. Ertl, T. Friedli, and S. D. Round, "PWM Converter Power Density Barriers," *Proc. Power Conversion Conference (PCC'07)*, Nagoya, Japan, April 2007, CD-ROM, ISBN: 1-4244-0844-X.

[3] J. A. Ferreira, and J. D. van Wyk, "Electromagnetic Energy Propagation in Power Electronic Converters: Toward Future Electromagnetic Integration," *Proc. IEEE*, vol. 89, pp. 876–889, June 2001.

[4] Q. Zhaoming, W. Xin, L. Zhengyu, and M. H. Pong, "Status of Electromagnetic Compatibility Research in Power Electronics," *Proc. Power Electronics and Motion Control Conf.*, vol.1, 2000, pp. 46-57.

[5] R. Redl, "Electromagnetic Environmental Impact of Power Electronics Equipment," *Proc. IEEE*, vol. 89, pp. 926–938, June 2001.

[6] M. J. Nave, *Power Line Filter Design for Switched-Mode Power Supplies*, New York, NY: Van Nostrand Reinhold, 1991.

[7] R. W. Erickson, and D. Maksimovic, *Fundamentals of Power Electronics*, 2nd ed., Norwell, Mass.: Kluwer Academic, 2001.

[8] A. Nagel, and R. W. De Doncker, "Systematic Design of EMI-Filters

for Power Converters," in *Proc. Industry Applications Conference*, vol. 4, 2000, pp. 2523-2525.

[9] P. Karutz, S. D. Round, M. L. Heldwein, and J. W. Kolar, "Ultra Compact Three-phase PWM Rectifier", *Proc. Applied Power Electron. Conf. (APEC'07)*, Anaheim, USA, Feb. 2007, pp. 816-822.

[10] G. Laimer, and J. W. Kolar, J.W, "'Zero'-Ripple EMI Input Filter Concepts for Application in a 1-U 500kHz Si/SiC Three-Phase PWM Rectifier," *Proc. International Telecom. Energy Conf. (INTELEC'03)*, Yokohama, Japan, Oct. 2003, pp. 750-756.

[11] W. Shen, F. Wang, D. Boroyevich, V. Stefanovic, and M. Arpilliere, "Optimizing EMI Filter Design for Motor Drives Considering Filter Component High-Frequency Characteristics and Noise Source Impedance", *Proc. Applied Power Electron. Conf. (APEC'04)*, vol.2, 2004, pp. 669-674.

[12] F. Barruel, J. L. Schanen, and N. Retiere, "Volumetric Optimization of Passive Filter for Power Electronics Input Stage in the More Electrical Aircraft," *Proc. Power Electron. Specialists Conf.*, Aachen, Germany, vol. 1, 2004, pp. 433-438.

[13] S. Chandrasekaran, S.A. Ragon, D. K. Lindner, Z. Gurdal, and D. Boroyevich, "Optimization of an Aircraft Power Distribution Subsystem". *AIAA Journal of Aircraft*, vol. 40, no. 1, pp. 16-26, 2003.

[14] European Center for Power Electronics, "The Industrial and Research Network for Power Electronics in Europe," Presentation ,2005. [Online] Available: http://www.ecpe.org.

[15] J. Miniböck, J. W. Kolar, and H. Ertl, "Design and Experimental Analysis of a 10kW Dual 400V/48V Interleaved Two-Transistor DC/DC Forward Converter System Supplied by a VIENNA Rectifier I," *Proc. Power Conversion / Intelligent Motion / Power Quality Conf.*, Nuremberg, Germany, June 2000, pp. 569-579.

[16] IEC International Special Committee on Radio Interference – C.I.S.P.R., "Information technology equipment – Radio disturbance characteristics – Limits and methods of measurement – Publication 22", Geneve, Switzerland: C.I.S.P.R, 1997.

[17] T. Nussbaumer, M. L. Heldwein, J. W. Kolar, "Differential Mode Input Filter Design for a Three-Phase Buck-Type PWM Rectifier Based on Modeling of the EMC Test Receiver," *IEEE Trans. on Industrial Electronics*, vol. 53, no. 5, 2006, pp. 1649-1661.

[18] International Electrotechnical Commission, "Safety of Information Technology Equipment – IEC 60950", Brussels, Belgium, 1999.

[19] Catalog, "Chip Monolithic Ceramic Capacitors," Murata. [Online]. Available: http://www.murata.com/catalog/c02e.pdf.

[20] M. J. Nave, "On Modeling the Common Mode Inductor," Symp. Electromagn. Compat. *(EMC'91)*, Aug 1991. pp. 452-457.

[21] W. G. Hurley, E. Gath, and J. G. Breslin, "Optimizing the AC resistance of multilayer transformer windings with arbitrary current waveforms," *Trans. Power Electron.*, vol. 15, no. 2, pp. 369-376, March 2000.

[22] Catalog, "Powder Cores Design Manual and Catalog," Magnetics. [Online]. Available: http://www.mag-inc.com/powder.

[23] Catalog, "Micrometals Catalog", Micrometals. [Online]. Available: http://www.micrometals.com.

[24] Catalog, "RFI Capacitors for the AC Line (X and Y capacitors)," Evox-Rifa. [Online]. Available: http://www.evoxrifa.com.

[25] R. D. Middlebrook, "Input Filter Considerations in Design and Application of Switching Regulators," *Proc. Industry Applications Society Annual Meeting*, Chicago (IL) USA, 1976, pp. 366-382.

[26] S. Y. Erich, and W. M. Polivka, "Input Filter Design Criteria for Current-Programmed Regulators," *Proc. Applied Power Electron. Conf. (APEC'90)*, Los Angeles, CA, USA, Mar. 1990, pp. 781-791.

[27] U. Drofenik, and J. W. Kolar, "Analyzing the Theoretical Limits of Forced Air-Cooling by Employing Advanced Composite Materials with Thermal Conductivities >400W/mK," *Proc. Conf. on Integrated Power Systems (CIPS'06)*, Naples, Italy, June 2006, pp. 323-328.

[28] M. L. Heldwein, T. Nussbaumer, F. Beck, and J. W. Kolar, "Novel Three-Phase CM/DM Conducted Emissions Separator," Proc. *Applied Power Electron. Conf. (APEC'05)*, Austin, Texas, USA, vol. 2, March 2005, pp. 797-802.

APPENDIX I – MINIMUM INDUCTANCE FOR A GIVEN ATTENUATION

The attenuation for the multi-stage LC filter of **Fig.18** is approximated for frequencies much higher than the cutoff frequency of the filter by,

$$Att(\omega)\big|_{\text{HF}} = \frac{U_2(\omega)}{U_1(\omega)} = \frac{1}{\omega^{2N} \cdot \prod_{j=1}^{N} L_j \cdot \prod_{j=1}^{N} C_j} . \quad (A.1)$$
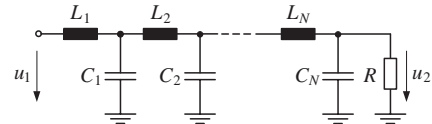

Fig.18: Multi-stage LC filter configuration.

Assuming that the capacitors C_j are known and that a given attenuation Att_{req} is required at a frequency ω_{req}, equation A.1 can be re rewritten,

$$\frac{1}{Att_{req} \cdot K_g} = \prod_{j=1}^{N} L_j , \text{ where } K_g = \omega_{req}^{2N} \cdot \prod_{j=1}^{N} C_j . \quad (A.2)$$

A maximum inductance L_{max} is defined as the sum of all inductors L_j,

$$L_{max} = \sum_{j=1}^{N} L_j . \quad (A.3)$$

Supposing that all inductors have the same value, then

$$L_j = \frac{L_{max}}{N} . \quad (A.4)$$

And the attenuation is given by,

$$\frac{1}{Att_{req} \cdot K_g} = \left(\frac{L_{max}}{N}\right)^N . \quad (A.5)$$

Having the premise that one of the inductors has a different value L_{dif}, defined by,

$$L_{dif} = \frac{k_{dif} \cdot L_{max}}{N}$$
$$L_j = L_{max} \cdot \frac{N - k_{dif}}{N \cdot (N-1)} , \text{ with } k_{dif} \geq 0 . \quad (A.6)$$

The attenuation equation for this new condition is,

$$\frac{1}{Att_{req} \cdot K_g} = \frac{k_{dif} \cdot (N-1)}{N - k_{dif}} \cdot \left(\frac{L_{dif} \cdot (N - k_{dif})}{K \cdot (N-1)}\right)^N . \quad (A.7)$$

Dividing equation A.7 by A.5 leads to the ratio $R(N,k_{dif})$ (cf. equation A.8) between the attenuation obtainable for both situations, which is graphically shown in **Fig.19**.

$$R(N, k_{dif}) = k_{dif} \cdot \left(\frac{N - k_{dif}}{N-1}\right)^{N-1} . \quad (A.8)$$

Differentiating $R(N,k_{dif})$ with respect to k_{dif},

$$\frac{\partial R(N, k_{dif})}{\partial k_{dif}} = -\frac{(N-1)(k_{dif} - 1)}{(k_{dif} - N)^2} \cdot \left(\frac{N - k_{dif}}{N-1}\right)^K . \quad (A.9)$$

Equating this result to zero leads to the maximum achievable attenuation,

$$\frac{\partial R(N, k_{dif})}{\partial k_{dif}} = 0 \Rightarrow k_{dif,optimum} = 1 . \quad (A.10)$$

As observed in equation A.10, k_{dif} equal to unity leads to the highest attenuation independent on the number of LC stages. That means that the maximum high frequency attenuation for a given L_{max} is achieved for equal components in all stages, since the structure of equation A.1 is the same for, both, inductances and capacitances.
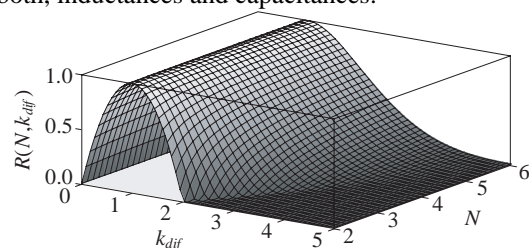

Fig.19: Ratio $R(N,k_{dif})$ between the attenuation obtainable with all inductors equal and the one for when a single inductor presents a different value.